axial fan noise: towards sound prediction based on numerical unsteady flow data - a case study

Hauke Reese[a] and Thomas Carolus[b]

[a]Ansys Germany GmbH, Birkenweg 14a, 64295 Darmstadt, Germany
[b]Institute of Fluid- and Thermodynamic, University of Siegen, Paul-Bonatz-Str. 9-11, 57068 Siegen, Germany
hauke.reese@ansys.com

A generic fan assembly consisting of a low pressure axial impeller including an optional turbulence generator is investigated. The flow field is simulated with different state-of-the-art unsteady computational fluid dynamic methods. All results are compared with each other and with hot wire flow velocity and surface pressure measurements. From the numerical data, the relevant dipole sound sources, i.e. the unsteady forces on the fan blades are derived. A free field formulation in the time domain (acoustical analogy by FFOWCS WILLIAMS and HAWKINGS), and a boundary element formulation in the frequency domain (SYSNOISE®) are employed to predict the radiated sound field based on the numerical source data. The acoustical results are compared and contrasted with measurements.

1 Introduction

Fans often operate under highly turbulent inflow conditions, e.g. due to their installation in a duct, downstream of struts or a radiator. This results in highly unsteady aerodynamic blade forces which in turn cause excessive sound radiation. Advanced state-of-the-art computational aero acoustic methods (CAA) allow increasingly reliable sound predictions. They usually require a detailed knowledge of the unsteady flow field, obtained by a simulation with a computational fluid dynamic method (CFD).

Ideally, a Direct Numerical Simulation (DNS) solves the Navier Stokes equation without further simplifications and predicts the unsteady flow and the corresponding acoustic field. However, a DNS is not feasible for a complex geometry such as a realistic fan because of its immense numerical costs. Finding the unsteady flow field with affordable efforts requires modelling at least parts of the turbulent fluctuations. Mainly two different strategies have been used to reduce the computational costs: (i) ensemble averaging which is known as the Unsteady Reynolds Averaged Navier Stokes Simulation (URANS) and (ii) filtering of the full Navier Stokes equations which leads to the Large Eddy Simulation (LES).

With URANS the reduction of computational costs is immense, the trade-off, however, is the large degree of approximation. All random turbulent fluctuations are modelled, thus only tonal sound sources of an axial flow fan can be predicted. A LES solves coarse turbulent structures directly and only small, high-frequency fluctuations are modelled. The numerical costs are still very high. To combine the advantages of a URANS with the higher resolution of a LES, hybrid methods like Detached Eddy Simulation (DES) or the Scale Adaptive Simulation (SAS) have been developed. The DES [1] combines a classical Reynolds averaged Navier Stokes simulation (RANS) with elements of a LES. The RANS method is applied in the near wall regions whereas the LES is active in detached flow regimes. The SAS is an improved URANS method. It has been developed by Menter et al [2, 3]. The key idea is to introduce the von Kárman length-scale into the turbulence scale equation and subsequently adjust dynamically the turbulence model as a function of the flow field, independent of the numerical grid.

The objective of the present paper is to investigate the capability of these different methods in terms of predicting gust noise sources of a rather complex technical object, a complete axial flow fan. For the investigation we have carried out four unsteady CFD simulations with URANS, SAS, DES and LES for a low pressure axial flow fan assembly with grid generated turbulent inflow. Eventually the sound radiation is predicted from the simulated sources by applying (i) FFOWCS WILLIAMS and HAWKINGS' analogy to the isolated impeller under free field conditions in the time domain and (ii) and with the casing as reflecting walls via a Boundary Element formulation in the frequency domain.

2 Fan assembly

The investigated fan impeller has a diameter of $D = 300$ mm and a hub/tip ratio $\nu = 0.45$. It is installed in a circular duct without guide vanes and rotates at $n = 3000$ rpm, resulting in a circumferential Mach number Ma = 0.14. The six cambered blades have a NACA 4509 profile. The Reynolds number, based on the chord length C of the blade and the mean relative flow velocity, varies from 118,000 at the hub to 178,000 at the tip. The radial tip clearance is 0.5 mm, which corresponds to 0.18 % of the rotor diameter D. The operating point of the maximum efficiency corresponds to a volumetric flow rate of $\dot{V} = 0.59$ m³/s. This operating point was selected for all the investigations in this study. A grid type turbulence generator is installed $0.56D$ upstream of the impeller's leading edge plane (hereafter, referred to as "reference plane", fig. 1). The turbulence generator consists of nine struts with a square cross-section of 15 x 15 mm² placed at a distance of 60 mm from each other.
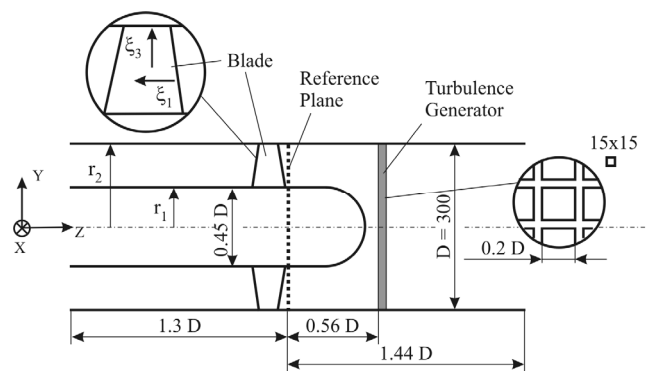

Fig.1 *Fan assembly with main flow from right to left*

3 Aerodynamic simulation

3.1 Numerical Methods

The numerical flow code employed throughout the LES is named FrontFlow/Blue. It has been developed by C. Kato and successfully used for several applications [4, 5]. The

code is based on a finite element discretization of the filtered incompressible continuity and Navier Stokes equations.

All other simulations are carried out with the commercial flow code ANSYS CFX10, which is based on a finite volume discretization. The URANS uses an implicit upwind differential scheme with a numerical advection correction which is formally of second order. The RANS part of the DES and SAS method is solved with same scheme. To avoid high numerical dissipation for the detached flow SAS and DES switch to a central difference scheme for such regions. The time integration is done by a second-order backward Euler scheme for all three methods. In the LES the sub grid scales (SGS) are modelled employing the dynamic Smagorinsky model proposed by Germano [6]. The shear stress transport model (SST) [7] in combination with an automatic wall function [8] is employed for the URANS. The DES and SAS are both set up on the SST model. A detailed description of the DES-SST formulation is given in [9] and for the SAS-SST formulation in [3].

3.2 Numerical Grid and Boundary Conditions

To meet the requirement of the different multiple frame interface capabilities of the two flow solvers and the different computational facilities two different hexahedral grids with basically the same structure (fig. 2) are used.

In order to ensure an acceptable simulation time, the leakage flow through the tip clearance is not taken into account. Also the overall number of the hexahedral elements for the entire flow domain is limited to approximately 5 millions for the LES. It is important to note that due to this limitation of grid resolution the *turbulent boundary layer* on the suction surface of the blades as well as on the casing wall will not be resolved by the LES. In the DES, SAS and URANS, only half of the impeller and the turbulence generator is meshed with approximately 1.5 million elements (fig. 2 right). This allows reducing the numerical costs while maintaining the same grid resolution.

For the LES a uniform axial velocity profile is set at the inlet. The mass flow, the direction of the velocity and a medium level of turbulence are defined as inflow conditions for all the other simulations. In all simulations we use a pressure outlet. In order to prevent reverse flow from the outlet boundary during the LES-iteration, a dummy section upstream of the outlet with a sudden expansion and a subsequent gradual contraction of the cross sectional area is installed. All remaining boundaries are set to no-slip wall condition.

The time increment Δt_{Solv} which is primarily determined by the stability limit of the simulation is set such that 10,000 time steps correspond to one single revolution of the impeller for the LES and 1,000 for all other simulations.
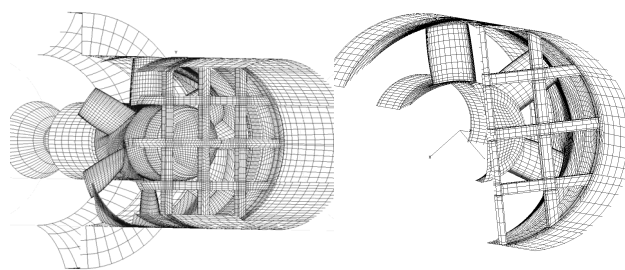

.Fig. 2 *Numerical grid; left: LES, right: URANS (only every third gridline is plotted)*

3.3 Aerodynamic Results

In order to verify the accuracy of the flow prediction in a first step the turbulence generator and the fan are investigated separately. The statistical parameters (turbulent intensity and correlation length) of flow downstream of the turbulence generating grid are in good agreement with hot wire measurements - for further details see [10, 11]. Looking at all predictions and evaluating the steady state fan design point the agreement with the experimental data is always better than 10% [11].

An illustrative aerodynamic result is the snapshot of the absolute velocity distribution in the complete assembly at a coaxial surface as depicted in Fig 3. The velocity distribution of the URANS is dominated by the wakes of the struts, which interact periodically with the impeller blades. Because of its high degree of turbulence modelling no coarse structures develop. By contrast the DES and SAS show turbulent structures from the wakes which move downstream and interact finally with the blades. Compared to the LES these structures are relatively coarse. Unfortunately in the LES some of the turbulent structures are destroyed numerically by the dynamical oversetting between the impeller and the turbulence generator grid.

Figure 4 depicts the predicted and measured [12] power spectral density levels of the wall pressure fluctuations $PSDL_{sp} = 10\log[d(\bar{p}_{sp}'^2 / df)/(p_0^2 / f_0)]$ dB on the blade suction-side due to the ingested inflow turbulence. The data have been evaluated at two monitoring points, one close to the leading edge (left side, P1) and one near mid-chord (right side, P2), both at approximately mid span. The predicted LES spectra are based on 10 impeller revolutions, all others on more than two revolutions after the flow field has become stationary in average. The power spectra from all simulated blades are averaged in order to reduce statistical uncertainties. At P1 (i.e. close to the leading edge) the predicted spectra show a satisfactory agreement with the measurements. Both, the predicted and the measured spectra show peaks at 200 and 400 Hz, which are clearly caused by the wakes of the upstream turbulence generator struts. These peaks are also well predicted by the URANS. The figure shows that SAS and DES can only predict pressure fluctuations lower than 1 kHz - the RANS in the boundary layer acts like a low pass filter. The LES predicts the pressure fluctuations up to 5 kHz.
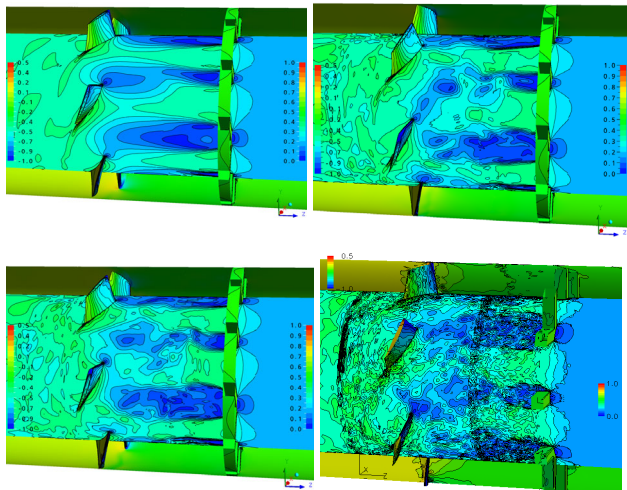
.Fig. 3 *Snapshot of the absolute velocity distribution normalized with the tip speed at midspan ($\xi_3 = 0,5$)*

(right-hand legend) and $C_p = \Delta p / (0.5\rho(D\pi n)^2)$ on all

body surfaces (left-hand legend); top left: URANS, top right: DES, bottom left: SAS, bottom right: LES
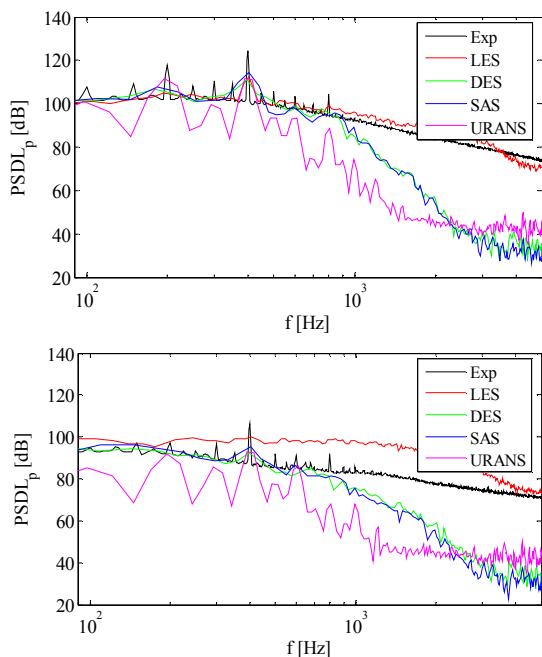

Fig. 4 *Comparison of the predicted and measured [20] power spectral density of the wall pressure fluctuations on the suction side at mid span, top: close to the leading edge (P1); bottom: mid chord (P2); (reference pressure $p_0 = 2 \ 10^{-5}$ Pa, reference frequency $f_0 = 1$ Hz).*

Comparing P2 with P1, the influence of the turbulent inflow ceases to exist. The level of the pressure fluctuations decreases in the downstream direction. All applied methods predict this behaviour well. However, the LES shows less satisfying results at P2 when compared to P1. The deviation is due to the fact that the grid is too coarse to resolve the turbulent boundary layer accurately. Artificial coarse structures are developing and cause higher levels of pressure fluctuations. Here DES and the SAS have a clear advantage. Because of their RANS inside the boundary layer regime, no over prediction of pressure fluctuation is observed.

4   Aeroacoustic Simulation

4.1   Methods

According to Curle [13] the sound radiation in a subsonic flow - as in the present case - is dominated by the dipole sound sources, which are caused by unsteady forces due to interaction of the flow with the moving surfaces. Employing a far field approximation the acoustical analogy of FFOWCS WILLIAMS and HAWKINGS [14] simplifies for the sound pressure p in an observer point **x** as

$$p(\mathbf{x},t) = \frac{1}{4\pi c_0} \int_{s(\tau)} \left[\frac{\mathbf{r}}{r^2 D} \frac{\partial}{\partial \tau} \frac{f_i}{|D|} \right]_{\tau e} ds(\sigma). \qquad (1)$$

Here D denotes a Doppler factor which takes the effect of the moving sources into account. c_0 is the speed of sound and **r** the place of the source in the relative coordinate system σ. The integral is solved at the retarded time τ and in the reference frame of the source.

The sound field under non free field conditions is predicted with the commercial program SYSNOISE®. The acoustical model is setup as a multi domain Direct Boundary Element Method (DBEM) where the sound pressure and velocity is represented on the boundary elements. Fig. 5 depicts the boundary element grid of the interior and the exterior domain. The coupling of the two domains takes place at the crossover of the inlet nozzle to the duct. The overall grid size of both domains is approximately 13,000 elements. This corresponds to a discretization of at least 6 elements per wave length up to a frequency of 1200 Hz. A non- reflecting boundary condition is set for both models on the cut surface downstream of the impeller. The sound sources of each blade are represented as a rotating dipole source in the model. A trick helps to implement all direct sound sources in SYSNOISE into account without loss of phase information: the impeller is split into six (LES) or three (SAS) impellers with one or two blades, respectively. The circumferential position of the superimposed artificial impellers is according to the full bladed impeller. In contrast to the free field method this model is setup in the frequency domain.
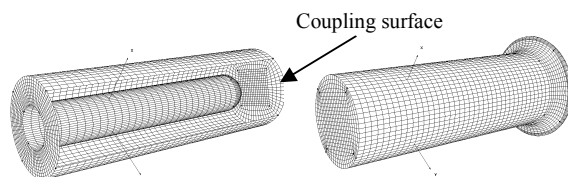

Fig. 5 *BEM-grid, left: internal grid, right external grid*

4.2   Aeroacoustic Results

The sound pressure is calculated at various observer points on a circle with a radius of one meter around the centre of the impeller (fig. 6).

Under free field conditions the inlet duct section is assumed acoustically transparent, which corresponds to the neglect of the short inlet section existing in the experiment [11]. The small difference of the microphone positions in the experiments and the position of the observer points with respect to the impeller is neglected. Fig. 9 shows the pre-

dicted and the measured power spectral density of the sound pressure $PSDL_{sp} = 10\log[d(\overline{p'_{sp}}^2 / df)/(p_0^2 / f_0)]$ dB

for two different observer points: on the rotational axis and at an angle of 45° to the rotational axis. With exception of the URANS based predictions, the results are in satisfactory agreement with the experimental data for both observer points. The spectra show that a standard URANS can only predict tonal sound. SAS and DES, however, are able to predict broad band noise up to a frequency of 1 kHz. LES yields acoustic predictions which are satisfactory up to 5 kHz in our test case.
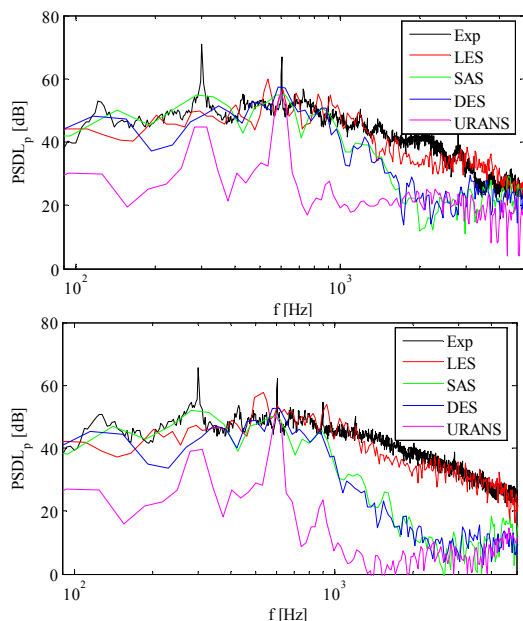

Fig.6 *Predicted sound pressure amplitude distribution; LES sources, left: BPF, right: 3xBPF*

Fig. 5 *Comparison of predicted and measured sound pressure power spectral density in a distance of one meter to the impeller centre point or the inlet nozzle; top: upstream of the rotational axis, bottom: upstream and at an angle of 45° to the rotational axis; (reference pressure $p_0 = 2\ 10^{-5}$ Pa, reference frequency $f_0 = 1\ Hz$)*

Fig.7 *Magnitude of the sound pressure power spectral density; top left: BPF, top right: 2xBPF, bottom left: 3xBPF, bottom right: 4xBPF*

However, as soon as the effect of the casing is important, the free field assumption is not valid any more.

The advantage of the DBEM method is depicted in fig. 6. The figure shows the sound pressure amplitude at blade passing frequency (BPF) and its third harmonic. At BPF the directivity is omni directional, whereas at 3x BPF the main radiation is at angles of 45° to the rotational axis. This is in good agreement with experimental data, fig. 7. Fig. 7 shows the directivity of the sound pressure for the BPF and the first four harmonics. Both, the measurements and the predicted directivities points out that the waves are guided by the duct only for smaller wave lengths. The predicted directivity patterns show a slight asymmetry. This might be due to the fact that the simulated time period is too short to get an averaged sound pressure power spectrum with a higher frequency resolution. One reason might be that the experimental setup includes effects which the simulations do not take into account; for example, some coarse structures could develop far upstream of the inlet nozzle due to the test environment, or the impeller is not perfectly balanced.
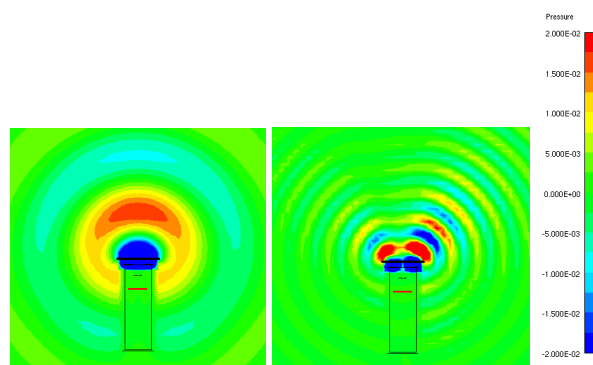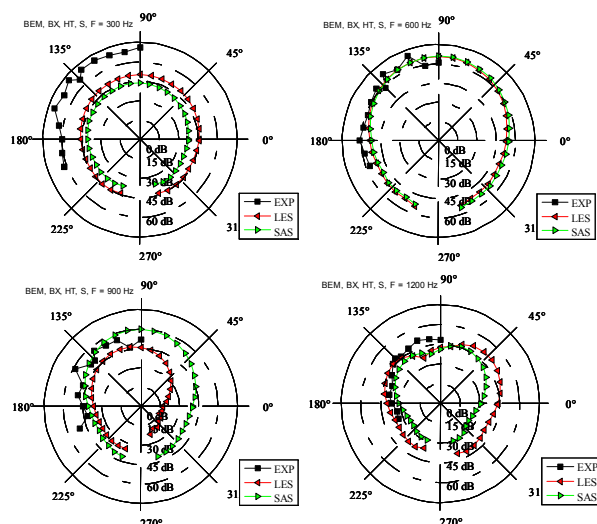
5   Conclusion

In this study LES, DES, SAS and URANS are tested to predict gust noise of a low pressure fan assembly with grid generated highly turbulent inflow. As compared to URANS, the SAS, DES and LES correctly predict the statistical parameters of the turbulence downstream of the turbulence generator resolving an increasing range of frequencies. The response of the blade leading edge region to the inflow turbulence in terms of surface pressure fluctuations is predicted accurately. The LES is capable of capturing pressure fluctuations up to a range of 5 kHz. One drawback of the LES are certainly the immense numerical costs.

The LES with its poor wall resolution tends to predict too strong wall pressure fluctuations towards the blade trailing edge which are attributed to numerical artefacts. The RANS within the SAS and DES method tends to suppress the development of such artificial structures because of its low pass filter effect. URANS can only predict tonal components of the pressure fluctuations caused by the wakes of the turbulence generator struts.

The characteristic of the sound field on the suction side, where the impeller more or less radiates into a free field, is predicted very well employing the Ffowcs Williams and Hawkings analogy fed from source data from the SAS, DES and LES. Again, only the LES was able to predict

sound up to realistically interesting frequencies up to 5 kHz. Although the source pressure fluctuations are in some regions over predicted, the overall acoustic prediction is found to be in good agreement with measurements. This is due to the fact that the level of the well predicted surface pressure (at the leading edge) dominates the overall acoustics by far.

The effect of the casing on the suction side sound field reflected better with the DBEM. The fundamental effects of the casing on to the sound radiation are well predicted. The radiation at higher frequencies is stronger influenced by the casing. Although the computational effort for the frequency domain DBEM is relatively low a drawback is the fact, that only discrete frequencies can be resolved. Time independent spectra with a high frequency resolution require long simulation times, which, however, are likely to become more and more realistic in the near future.

Acknowledgments

References

[1] P.R. Spalart, W.H. Jou, M. Strelets, S.R. Allmaras, " Comments on the Feasibility of LES for Wings and on a Hybrid RANS/LES Approach". *1st AFOSR Int. Conf. On DNS/LES Ruston LA, In Advances in DNS/LES C. Lui & Z. Liu Eds., Greyden Press, Columbus, OH* (**1997**)

[2] F. Menter, M. Kuntz, R. Bender, „A Scale Adaptive Simulation Model for Turbulent Flow Predictions", *AIAA Paper,* AIAA2003-0767 (**2003**)

[3] F.R. Menter, Y. Egorov, "A Scale-Adaptive Simulation Model Using Two-Equation Models", *AIAA Paper,* AIAA2005-1095 (**2005**)

[4] C. Kato, H. Mukai and A. Manabe, "Large Eddy Simulation of Unsteady Flow in a Mixed-Flow Pump", *The 9th International Symposium on Transport Phenomena and Dynamics of Rotating Machinery, Honolulu, Hawaii* (**2002**)

[5] C. Kato, M. Kaiho and A. Manabe, "An Overset Finite Element Large Eddy Simulation Method with Application to Turbomachinery and Aeroacoustics", *J. Appl. Mech.,* 70, 32-43 (**2003**)

[6] M. Germano, U. Poimelli, P. Moin and W. H. Cabot, "A Dynamic Subgrid-Scale Eddy Viscosity Model", *Phys. Fluids,* A3(7), 1760-1765 (**1991**)

[7] F. Menter, "Two-Equation Eddy-Viscosity Turbulence Models for Engineering Applications", *AIAA Journal,* 32(8), 1598-1605 (**1994**)

[8] F. Menter, T. Esch, "Elements of Industrial Heat Transfer Predictions", *16th Brazilian Congress of Mechanical Engineering (COBEM), Uberlandia, Brazil* (**2001**)

[9] F. Menter, M. Kuntz, "Development and Application of a Zonal DES Turbulence Model for CFX-5" , *ANSYSY CFX Validation Report,* CFX-VAL17/0404 (**2004**)

[10] M. Schneider, „Der Einfluss der Zuströmbedingungen auf das breitbandige Geräusch eines Axialventilators", *Fortschr.-Ber.* VDI Reihe 7, Nr. 478, VDI Verlag, Düsseldorf (**2006**)

[11] H. Reese, „Anwendung von instationären numerischen Simulationsmethoden zur Berechnung aeroakustischer Schallquellen bei Axialventilatoren, Fortschr.-Ber. VDI Reihe 7, Nr. 489, VDI Verlag, Düsseldorf (**2007**)

[12] T. Carolus and M. Stremel, "Blade Surface Pressure Fluctuations and Acoustic Radiation from an Axial Fan Rotor Due to Turbulent Inflow",. *Acta Acustica United With Acoustica,* 88, 472-482 (**2002**)

[13] N. Curle, "The Influence of Solid Boundaries Upon Aerodynamic Sound", *Proc. R. Soc. London,* 211, Series A, 505-514 (**1955**)

[14] J. E. Ffowcs Williams, D. L. Hawkings, "Sound generation by turbulence and surfaces in arbitrary motion", *Phil. Trans. Ryo. Soc.,* A264 (**1969**)